

A Numerical Study on Hydraulic Fracturing Problems via the Proper Generalized Decomposition Method

Daobing Wang^{1,*}, Sergio Zlotnik^{2,*}, Pedro Díez², Hongkui Ge³, Fujian Zhou³ and Bo Yu⁴

Abstract: The hydraulic fracturing is a nonlinear, fluid-solid coupling and transient problem, in most cases it is always time-consuming to simulate this process numerically. In recent years, although many numerical methods were proposed to settle this problem, most of them still require a large amount of computer resources. Thus it is a high demand to develop more efficient numerical approaches to achieve the real-time monitoring of the fracture geometry during the hydraulic fracturing treatment. In this study, a reduced order modeling technique namely Proper Generalized Decomposition (PGD), is applied to accelerate the simulations of the transient, non-linear coupled system of hydraulic fracturing problem, to match this extremely tight response time constraint. The separability of the solution in space and time dimensions is studied for a simplified model problem. The solid and fluid equations are coupled explicitly by inverting the solid discrete problem, and a simple iterative procedure to handle the non-linear characteristic of the hydraulic fracturing problem is proposed in this work. Numerical validation illustrates that the results of PGD match well with those of standard finite element method in terms of fracture opening and fluid pressure in the hydro-fracture. Moreover, after the off-line calculations, the numerical results can be obtained in real time.

Keywords: Hydraulic fracturing, proper generalized decomposition, reduced order modeling, numerical simulation.

1 Introduction

Hydraulic fracturing, also termed as hydro-fracking, is a very important technology in the petroleum industry because it can obviously stimulate more production of oil and gas wells [Yew and Weng (2014); Wang, Shahvali and Su (2015)]. Recently, with advances in these technologies such as horizontal well drilling and segregated completion, hydraulic

¹School of Mechanical Engineering, Beijing Key Laboratory of Pipeline Critical Technology and Equipment for Deepwater Oil & Gas Development, Beijing Institute of Petrochemical Technology, Beijing, 102617, China.

²Laboratori de Càlcul Numèric (LaCàN), ETS de Ingeniero de Caminos, Canales y Puertos, Universitat Politècnica de Catalunya, Barcelona, E-08034, Spain.

³Research Institute of Unconventional Oil and Gas Science and Technology, China University of Petroleum, Beijing, 102249, China.

⁴Department of Oil & Gas Transportation and Engineering, Beijing Institute of Petrochemical Technology, Beijing, 102617, China.

*Corresponding Authors: Daobing Wang. Email: upcwdb@bipt.edu.cn;
Sergio Zlotnik. Email: sergio.zlotnik@upc.edu.

Received: 22 July 2019; Accepted: 08 October 2019.

fracturing has become an essential part of commercially developed unconventional hydrocarbon reservoirs, such as shale gas, coal-bed methane, deep geothermal resources and tight hydrocarbon reservoirs. All the time, the determination of the fracture geometry and propagation path in hydraulic fracturing has been a research hotspot in petroleum engineering [Nolte and Economides (2000)]. However, the numerical simulation of hydro-fracking problem is a time-consuming task due to the strongly non-linear coupling between the equations for the fluid flow in the hydro-fracture and rock deformation. To handle this hydro-mechanical coupled problem, various numerical methods have been successfully put forward in recent years [Hunsweck, Shen and Lew (2013); Yuan, Zheng, Moghanloo et al. (2017); Kumar, Camilleri and Brewer (2016); McClure, Babazadeh, Shiozawa et al. (2016)].

These numerical methods have been successfully applied in the simulation of hydraulic fracturing, which are involved in finite difference method (FDM), finite element method (FEM), extended finite element method (XFEM), discrete element method (DEM), and numerical manifold method (NMM), etc. For the first two methods, their solutions will depend on the mesh size near the hydraulically-driven fractures because of the stress singularity in the vicinity of crack tips [Pogacnik, Elsworth, O'Sullivan et al. (2016); Yan and Zheng (2017); Shimizu, Murata and Ishida (2011); Douillet-Grellier, Pramanik, Pan et al. (2016)]. DEM offers more advantages than other numerical methods in the simulation of discontinuous problems, but most of the simulation time is occupied in the explicit iteration of small time step and contact judgment between two adjacent elements [Pogacnik, Elsworth, O'Sullivan et al. (2016)]. For XFEM, the calculated crack can freely propagate that is independent on mesh sizes because additional enrichment functions are introduced into the standard shape functions. However, the enrichment process will take up most of central processing unit (CPU) time, and thus it is difficult to simulate complex fracture networks [Shimizu, Murata and Ishida (2011); Haddad, Du and Vidal-Gilbert (2017)]. Therefore, these mentioned methods are time-consuming in the simulation of hydro-fracking problem because we have to deal with the same above-mentioned difficulties: non-linear, transient and coupled. It will take so much time, normally several hours to days, to simulate the fracture propagation process on a computer, therefore it still remains a great challenge to predict the fracture geometry in real time during the fracking operations [Shimizu, Murata and Ishida (2011); Douillet-Grellier, Pramanik, Pan et al. (2016); Mieke and Mauthe (2016); Haddad and Sepehrnoori (2015); Adachi, Siebrits, Peirce et al. (2007); Ji, Settari and Sullivan (2009)].

In order to efficiently solve this difficulty, the new idea is to solve the non-linear, transient and coupled partial differential equations (PDEs) via model order reduction method (ROM) such as Proper Orthogonal Decomposition method (POD) or Reduced Basis (RB) method [Secchi and Schrefler (2012); Chinesta, Keunings and Leygue (2013); Chinesta, Ladeveze and Cueto (2011); González, Alfaro, Quesada et al. (2015); Henneron and Clenet (2015)]. Model order reduction aims to reduce the computational complexity by means of a reduction of the associated state space dimension or degrees of freedom. The Proper Generalized Decomposition (PGD) method, a kind of novel ROM method, is firstly introduced by French mathematician Pierre Ladevèze et al. [Chinesta, Ladeveze and Cueto (2011); Ladevèze, Passieux and Néron (2010)]. In the PGD framework, the solutions are represented by several independently separated functions. It means that PGD method can successfully separate the time and space domain for transient PDEs, and thus the original

time-dependent problem is divided into 1D time problem and 2D or 3D space problem. And then alternating fixed strategies are adopted to solve the non-linear and coupled problem with a relatively low computational cost in an enrichment process. Recently, PGD method has been successfully applied in many challenging issues involved in various fields of science and engineering [Signorini, Zlotnik and Díez (2017); Aguado, Huerta, Chinesta et al. (2015)], and it is proved to be a more efficient and powerful algorithm [Aguado, Huerta, Chinesta et al. (2015); Ammar (2010); Zlotnik, Díez, Modesto et al. (2015); Tamellini, Le Maitre and Nouy (2014)].

In this paper, the PGD method is firstly applied in hydraulic fracturing problems to achieve the fast simulation of the fracture geometry. Firstly, the singular valued decomposition (SVD) method is used to linearize the cubic term of PDEs, then the fast PGD solver is constructed to separate the time domain and space domain to reduce the associated dimensions, and finally get the fracture geometry in a real-time mode. Verification test is carried out by the comparison of results between PGD and FEM. This new PGD solver will be much more useful and attractive for simulating the hydraulic fracturing problem within the oil and gas industry in the future.

2 Problem statement

To simply the construction of PGD-ROM, the following assumptions are made without loss of generality: (1) the hydraulic fracturing treatment is considered to be a two-dimensional plane strain problem; (2) there is almost no fluid leak-off normal to the fracture wall because of the low matrix permeability; (3) the injection fluid is Newtonian fluid, and thus the viscosity is assumed as a constant in hydraulic fracturing; (4) it is an isothermal process during the hydraulic fracturing, and thus the fracturing fluid viscosity is independent on the temperature.

2.1 Governing equations

The governing equations of hydro-fracking problem are composed of two coupled equations: the classical stress equilibrium equation representing rock deformation, and the transient fluid flow equation in the hydraulically-driven fracture [Yew and Weng (2014)].

2.1.1 Stress equilibrium equation

Based on the classical theory of linear elasticity, the solid part of hydro-fracking PDEs consists in stress equilibrium equation and proper boundary conditions [Yew and Weng (2014); Nolte and Economides (2000)] finding a displacement function $u(x, y)$ taking values in a 2D domain of Ω , as shown in Fig. 1, such that

$$\nabla \cdot \sigma = 0 \quad \text{in } \Omega \quad (1)$$

$$\sigma \cdot n_t = \sigma_H \quad \text{on } \Gamma_L \cup \Gamma_R \quad (2)$$

$$\sigma \cdot n_t = \sigma_h \quad \text{on } \Gamma_T \cup \Gamma_B \quad (3)$$

$$\sigma \cdot n_f = p(s, t) \quad \text{on } \Gamma_f \quad (4)$$

$$u = 0 \quad \text{at the four corner points} \quad (5)$$

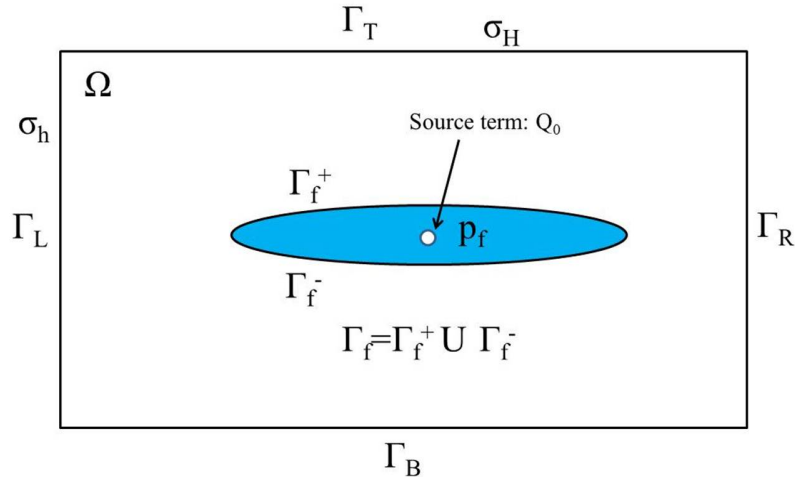


Figure 1: Schematic of HF propagation. $\Gamma_{out} = \Gamma_L \cup \Gamma_R \cup \Gamma_T \cup \Gamma_B$ denotes the outer boundary, and fracture wall $\Gamma_f = \Gamma_f^+ \cup \Gamma_f^-$ denotes the inner boundary, where the superscript symbol + and – are respectively the upper and lower fracture surface

where Eq. (1) denotes the stress equilibrium equation, and Eqs. (2)-(5) denote its boundary conditions; σ denotes the second-order Cauchy stress tensor; u denotes the displacement tensor vector; $p(s, t)$ denotes the fluid pressure scalar acted on the fracture wall Γ_f ; σ_H and σ_h respectively denote the maximum and minimum horizontal principal stress in the far field; n_t and n_f respectively denote the normal unit vector, which is perpendicular to the outer boundary $\Gamma_{out} = \Gamma_L \cup \Gamma_R \cup \Gamma_T \cup \Gamma_B$ and inner boundary Γ_f ; s denotes the space variable representing crack positions; t denotes the injection time.

Under the condition of elastic deformation, the constitutive equation between stress tensor and strain tensor can be represented as [Yew and Weng (2014); Hunsweck, Shen and Lew (2013)]:

$$\sigma_e = D : \varepsilon \quad (6)$$

where σ_e denotes the effective stress tensor; ε denotes the second-order strain tensor; D denotes a fourth-order elastic stiffness tensor. If isotropic rock is under plane strain conditions, D is a 3×3 square matrix:

$$D = \frac{E}{1 - \nu^2} \begin{bmatrix} 1 & \nu & 0 \\ \nu & 1 & 0 \\ 0 & 0 & \frac{1-\nu}{2} \end{bmatrix} \quad (7)$$

where E denotes Young's modulus, and ν denotes Poisson's ratio.

Under small-deformation assumption, there is a linear relationship between strain tensor and displacement vector [Yew and Weng (2014); Fjar, Holt, Raaen et al. (2008)],

$$\varepsilon = \nabla^s u = \frac{1}{2}(\nabla u + \nabla u^T) \quad (8)$$

where ∇^s denotes the symmetric operator.

According to the Terzaghi-Biot effective stress principle, Cauchy stress can be divided into two parts [Fjar, Holt, Raaen et al. (2008)]:

$$\sigma_e = \sigma - \alpha p_p \tag{9}$$

where p_p denotes the pore pressure acted on rock skeletons; α denotes Biot elastic coefficient, $\alpha \in [0, 1]$.

2.1.2 Fluid flow equation

According to the lubrication theory in fluid mechanics, the continuity equation of a planar Poiseuille flow between two parallel plates satisfies [Yew and Weng (2014); Nolte and Economides (2000)]:

$$\frac{\partial w}{\partial t} = \frac{\partial}{\partial s} \left(k \frac{\partial p}{\partial s} \right) + Q_0 \quad \text{in } \Omega_f \tag{10}$$

$$k = \frac{w^3}{12\mu} \tag{11}$$

$$w = (u^+ - u^-) |_{\Gamma_f} \tag{12}$$

$$\frac{w^3}{12\mu} \frac{\partial p}{\partial n} = 0 \quad \text{on two crack tips} \tag{13}$$

where w denotes the fracture width; μ denotes the viscosity of fracturing fluid; Q_0 denotes the source term, i.e., injection point; k denotes the fracture permeability; Ω_f denotes the crack surface. It should be mentioned that Eq. (10) is a non-linear equation because of the cubic term w^3 , i.e., the coefficient of the second derivative. According to Eq. (13), it shows that the fluid flow equation satisfies the Neumann boundary condition at the two crack tips. In Eq. (12), the superscripts “+” and “-” denote the two fracture surfaces of Ω_f .

According to Eq. (12), there is a certain sparse geometry matrix A , such that

$$w = Au |_{\Omega} \tag{14}$$

For each row in matrix A , the only two non-zero entities are equal to 1 or -1, and others are all equal to zero. Eq. (14) smoothly builds the connection between displacement field u in domain Ω and fracture width field w in domain Ω_f .

2.2 Weak forms

According to the variational principles for stress equilibrium equation and fluid flow equation, the trial solution spaces of displacement and fluid pressure fields are respectively defined as follows:

$$\mathfrak{S}_u = \{u \in [H^1(\Omega; C)]^2 \mid u = 0 \text{ on } \Gamma_{\text{out}}\} \tag{15}$$

$$\mathfrak{S}_p = \{p \in [H^1(\Omega_f; C)] \mid p = 0 \text{ on } \Gamma_f\} \tag{16}$$

where H^1 denotes Hilbert space.

In the above definitions, the two sets (15) and (16) satisfy with Dirichlet boundary conditions of solid part Eq. (1) and fluid part Eq. (10). After multiplying the weighted functions δ_u and δ_p on two sides of Eqs. (1) and (10), and integral by parts, their

corresponding weak forms can be expressed as Eqs. (17) and (18). Its statement is as follows: find $(u, p) \in \mathfrak{S}_u \times \mathfrak{S}_p$ such that for all $(\delta u, \delta p)$

$$\int_{\Omega} \delta \varepsilon^T \sigma d\Omega - \int_{\Gamma_{out}} \delta u^T \sigma_0 d\Gamma + \int_{\Omega_f} (\delta u^{+T} - \delta u^{-T}) p d\Omega_f = 0 \quad (17)$$

$$\int_{\Omega_f} \delta p w d\Omega_f + \int_{\Omega_f} \nabla(\delta p) \frac{w^3}{12\mu} \nabla p d\Omega_f + \int_{\Omega_f} \delta p Q_0 d\Omega_f = 0 \quad (18)$$

where σ_0 is equal to σ_H or σ_h on the outer boundary Γ_{out} [Hunsweck, Shen and Lew (2013); Adachi, Siebrits, Peirce et al. (2007)].

3 Numerical methods

3.1 FEM formulation

Assume that N_i^u and N_i^p respectively denote the nodal displacement and fluid pressure shape functions, u_i and p_i respectively denote the nodal displacement and fluid pressure value, N_u and N_p respectively denote the vector of nodal displacement and fluid shape functions, \tilde{u} and \tilde{p} respectively denote the vector of nodal displacement and fluid pressure. Then the displacement and fluid pressure field are respectively expressed as: $u \approx u^h = \sum_{i=1}^{n_u} N_i^u u_i = N_u \tilde{u}$, $p \approx p^h = \sum_{i=1}^{n_p} N_i^p p_i = N_p \tilde{p}$ in discrete forms.

3.1.1 The discretization of stress field equation

According to Galerkin FEM method, the discrete form of Eq. (17) is represented as follows:

$$K_s \tilde{u}^{n+1} - M_s \tilde{p}^{n+1} - f_s = 0 \quad (19)$$

where K_s denotes the stiffness matrix, $K_s = \int_{\Omega} B^T D B d\Omega$; f_s denotes the load vector of solid part; $f_s = \int_{\Gamma_{out}} N_u^T \sigma_0 d\Gamma$; M_s denotes the coupling matrix between solid and fluid parts; $M_s = \int_{\Omega_f} N_u^T N_p d\Omega_f$; and B denotes the geometry matrix that represents the relationship between displacement and strain for each element.

3.1.2 The discretization of fluid flow equation

Before getting the discrete form of fluid part, substituting Eq. (14) into the weak form of fluid problem (18) yields,

$$\int_{\Omega_f} \delta p A \dot{u} d\Omega_f + \int_{\Omega_f} \nabla(\delta p) k \nabla p d\Omega_f + \int_{\Omega_f} \delta p Q_0 d\Omega_f = 0 \quad (20)$$

Similar to the above-mentioned process of solid part, substituting $\delta p = N_p$, $p = N_p \tilde{p}$, $u = N_u \tilde{u}$ into the above weak form, and then the discretization scheme of its weak form is obtained as follows:

$$M_f A \dot{\tilde{u}}^{n+1} + K_{f(w^3)} \tilde{p}^{n+1} - f_f = 0 \quad (21)$$

where $\dot{\tilde{u}}$ denotes the first order time derivative of \tilde{u} ; \tilde{u}^{n+1} is the nodal displacement in domain Ω at time $n + 1$; $M_f = (M_s)^T = \int_{\Omega_f} (N_p)^T N_u d\Omega_f$; K_f denotes the permeability matrix; $K_{f(w^3)} = \int_{\Omega_f} (\nabla N_p)^T k(\nabla N_p) d\Omega_f = \int_{\Omega_f} (\nabla N_p)^T \frac{w^3}{12\mu} (\nabla N_p) d\Omega_f$; f_f denotes the load vector of fluid part; $f_f = \int_{\Omega_f} (N_p)^T Q_0 d\Omega_f$.

To discretize the discretization of time derivative term in Eq. (21), backward finite difference is adopted to approximate the time derivative of displacement \tilde{u} in Eq. (21).

$$\dot{\tilde{u}}^{n+1} = \frac{\tilde{u}^{n+1} - \tilde{u}^n}{\Delta t} \tag{22}$$

$$M_f A \frac{\tilde{u}^{n+1}}{\Delta t} + K_{f(w^3)} \tilde{p}^{n+1} - f_f - M_f A \frac{\tilde{u}^n}{\Delta t} = 0 \tag{23}$$

where n denotes the n -th time layer. The cubic term w^3 in the integral of $K_{f(w^3)}$ makes Eq. (24) to be a nonlinear equation.

Finally the fully coupled solid-fluid forms between Eq. (19) and Eq. (23) can be expressed in the block matrix form:

$$\begin{bmatrix} K_s & -M_s \\ \frac{1}{\Delta t} M_f A & K_{f(w^3)} \end{bmatrix} \begin{bmatrix} \tilde{u}^{n+1} \\ \tilde{p}^{n+1} \end{bmatrix} = \begin{bmatrix} f_s \\ f_f + \frac{1}{\Delta t} M_f A \tilde{u}^n \end{bmatrix} \tag{24}$$

where \tilde{u}^{n+1} and \tilde{u}^n respectively denotes the displacement at the time $n + 1$ and n .

3.2 PGD formulation

3.2.1 Preliminary treatment

According to the discrete form of solid part Eq. (19), the displacement function u can be expressed as:

$$u(x, t) = K_s^{-1} f_s + K_s^{-1} M_s p(x, t) = b + B \cdot p(x, t) \tag{25}$$

where $b = K_s^{-1} f_s$, and $B = K_s^{-1} M_s$. Substituting the above equation into Eq. (14) and Eq. (23), we obtain

$$w(x, t) = Au(x, t) = A(Bp + b) \tag{26}$$

$$\dot{w} = AB\dot{p} \tag{27}$$

$$M_f AB\dot{p} + K_{f(w^3)} p = Q_0 \tag{28}$$

For simplicity, the subscript “ f ” is ignored in the next section without any ambiguity. Eq. (26) indicates us that once the separated forms of pressure solution of Eq. (28) is obtained, it is easy to get the PGD solutions of displacement and crack opening according to Eqs. (25) and (26). Here, it should be mentioned that the vector b and matrix B in Eq. (25) are only the function of space variable. Thus, the next step is only to seek for the PGD solution of fluid part by means of inverting the discrete form of solid part.

3.2.2 The separated representation of the coupled system

The separated representations of PGD of fluid problem are as follows [Chinesta, Keunings and Leygue (2013); Chinesta, Ladeveze and Cueto (2011)]:

$$p^m(x, t) = \sum_{i=1}^m X_i(x)T_i(t) = p^{m-1}(x, t) + X(x)T(t) \quad (29)$$

where m denotes the modes of separated terms; X and T are unknowns at current enrichment step m ; p^{m-1} is the first $m-1$ terms of PGD form, which is already computed. Here again for simplicity, the subscript symbol “ m ” is neglected instead of X, T without any ambiguity.

Substituting Eq. (29) into Eq. (28) yields,

$$MABX(x)\dot{T}(t) + K_{w^3}X(x)T(t) = Q_0 - MABp^{m-1} - K_{w^3}p^{m-1}$$

Because of the non-linear term K_{w^3} , here SVD method is used to separate the matrix into space domain and time domain [Chinesta, Keunings and Leygue (2013); Chinesta, Ladeveze and Cueto (2011)].

$$[K_{w^3}]_{ij} = \int_{\Omega_f} N_i \frac{w^3}{12\mu} N_j ds \quad (30)$$

$$\frac{w^3(x, t)}{12\mu} \simeq \sum_l \theta^l(x)\phi^l(t) \quad (31)$$

$$K_{w^3} \simeq \sum_l K^l \phi^l(t) \quad (32)$$

where $[K^l]_{ij} = \int_{\Omega_f} N_i \theta^l(x) N_j dx$. Now our expected separated forms of fluid problem are formulated as:

$$MABX(x)\dot{T}(t) + \sum_l K^l \phi^l(t) X(x)T(t) = Q_0 - MABp^{m-1} - \sum_l K^l \phi^l(t) p^{m-1} \quad (33)$$

3.3 Alternating direction iteration

At enrichment step m , both functions X and T are unknown at the current enrichment step. Their product $X \cdot T$ makes the equation nonlinear. Thus herein alternating direction iteration is utilized to handle the non-linear problem. This kind of iterative scheme includes two steps for each iteration step p : (1) given $T_m^{p-1}(t)$, compute $X_m^p(x)$; (2) given the just-computed $X_m^p(x)$, compute $T_m^p(t)$. At the beginning of iteration, a random vector guess T_m^0 is specified. The stopping criterion of alternating direction iteration is defined as follows [Chinesta, Keunings and Leygue (2013); Chinesta, Ladeveze and Cueto (2011); Signorini, Zlotnik and Díez (2017); Aguado, Huerta, Chinesta et al. (2015)]:

$$\frac{\| X_m^p(x)T_m^p(t) - X_m^{p-1}(x)T_m^{p-1}(t) \|}{\| X_m^{p-1}(x)T_m^{p-1}(t) \|} < \varepsilon \quad (34)$$

where $\| \cdot \|$ is the L2-norm, and ε is a specified tolerance. Once the computed $X_m^p(x)$ and $T_m^p(t)$ satisfy the criterion, both of them will be assigned to $X_m(x)$ and $T_m(t)$ respectively. In following, the superscript of iterative step p is also again neglected for simplicity without any ambiguity.

• Given T , Calculate X

Since all functions of t are known, T is multiplied on both sides of Eq. (34) and then carry out the integration in time domain. It means that given T , find X such that

$$\int_{\Omega_{time}} T[MABX\dot{T} + \sum_l K^l \phi^l(t)XT]dt = \int_{\Omega_{time}} T[Q_0 - MAB\dot{p}^{m-1} - \sum_l K^l \phi^l p^{m-1}]dt \tag{35}$$

$$[MAB \int_{\Omega_{time}} T\dot{T}dt + \sum_l K^l \int_{\Omega_{time}} T\phi^l Tdt]X = Q_0 \int_{\Omega_{time}} Tdt - \sum_{i=1}^{m-1} MABX_i$$

$$\int_{\Omega_{time}} T\dot{T}_i dt - \sum_{i=1}^{m-1} \sum_l K^l X_i \int_{\Omega_{time}} T\phi^l T_i dt \tag{36}$$

In the above expression, the following coefficients associated with 1D integral over Ω_{time} are defined as:

$$\alpha^x = \int_{\Omega_{time}} T\dot{T}dt \tag{37}$$

$$\beta^{x,l} = \int_{\Omega_{time}} T\phi^l Tdt \tag{38}$$

$$\gamma^x = \int_{\Omega_{time}} Tdt \tag{39}$$

$$\alpha_i^x = \int_{\Omega_{time}} T\dot{T}_i dt \tag{40}$$

$$\beta_i^{x,l} = \int_{\Omega_{time}} T\phi^l T_i dt \tag{41}$$

Therefore the compact form of our final seeking function X is expressed as:

$$(MAB\alpha^x + \sum_l K^l \beta^{x,l})X = Q_0\gamma^x - \sum_{i=1}^{m-1} MABX_i\alpha_i^x - \sum_{i=1}^{m-1} \sum_l K^l X_i\beta_i^{x,l} \tag{42}$$

The strong form of the Boundary Value Problem (BVP) is an algebra equation of X , it can be numerically solved by means of any appropriate numerical methods.

• Given X , Calculate T

Similar to the above procedure, since all functions of x are known, X^T is multiplied on both sides of Eq. (34). It means that given X , find T such that

$$X^T[MABX\dot{T} + \sum_l K^l \phi^l XT] = X^T[Q_0 - MAB\dot{p}^{m-1} - \sum_l K^l \phi^l p^{m-1}](X^T MABX)\dot{T}$$

$$+ \sum_l X^T K^l X\phi^l T = X^T Q_0 - \sum_{i=1}^{m-1} X^T MABX_i\dot{T}_i - \sum_{i=1}^{m-1} \sum_l X^T K^l X_i\phi^l T_i \tag{43}$$

In the above expression, the following coefficients dependent on space variable x are defined as:

$$\alpha^t = X^T M A B X \quad (44)$$

$$\beta^{t,l} = X^T K^l X \quad (45)$$

$$\gamma^t = X^T Q_0 \quad (46)$$

$$\alpha_i^t = X^T M A B X_i \quad (47)$$

$$\beta_i^{t,l} = X^T K^l X_i \quad (48)$$

$$\xi^t = \gamma^t - \sum_{i=1}^m \alpha_i^t \dot{T}_i - \sum_{i=1}^{m-1} \sum_l \beta_i^{t,l} \phi^l T_i \quad (49)$$

Thus the compact form of Eq. (44) is formulated as:

$$\alpha^t \dot{T} + \sum_l \beta^{t,l} \phi^l T = \xi^t \quad (50)$$

$$\dot{T} = (\gamma - \sum_l \beta^{t,l} \phi^l T) \frac{1}{\alpha^t} \quad (51)$$

$$F(t, T) = (\xi^t - \sum_l \beta^{t,l} \phi^l T) \frac{1}{\alpha^t} \quad (52)$$

The strong form of the Initial Value Problem (IVP) is a first-order ordinary differential equation (ODE) of T , it can be numerically solved by means of the fourth-order Runge-Kutta (RK4) method. Assume initial condition $T(0) = 0$, and use RK4 scheme, we get:

$$T_{i+1} = T_i + \frac{\Delta t}{6} (k_1 + 2k_2 + 2k_3 + k_4) \quad (53)$$

$$k_1 = F(t_i, T_i) \quad (54)$$

$$k_2 = F(t_i + \frac{\Delta t}{2}, T_i + \frac{\Delta t}{2} k_1) \quad (55)$$

$$k_3 = F(t_i + \frac{\Delta t}{2}, T_i + \frac{\Delta t}{2} k_2) \quad (56)$$

$$k_4 = F(t_i + \Delta t, T_i + \Delta t k_3) \quad (57)$$

3.4 Linearized strategy

In the previous section, the matrix K_{w^3} is non-linear, therefore Picard iterative method (i.e., fixed point method) is used to solve and linearize the discrete system of Eq. (27). The corresponding iterative scheme is [Yew and Weng (2014)]:

$$M A B \dot{p}^{\delta+1} + K_{w^3}^\delta p^{\delta+1} = Q_0 \quad (58)$$

where δ denotes the Picard iteration number. When it satisfies the stopping criterion: $\|p^{\delta+1} - p^\delta\| < \epsilon$, the final p will be obtained.

3.5 Algorithm summary

The assumptions of hydro-fracking model are as follows: (1) there is no fluid leak-off rate on fracture surfaces, and thus fluid flow can be considered into a pure 1D problem along the fracture length; (2) the complicated 3D stress field can be simplified as a 2D plain strain problem because of the great thickness of the reservoir; (3) The fracturing fluid is Newtonian fluid, and thus the fluid viscosity will be kept a constant in hydraulic fracturing; (4) a hydro-fracture will extend along a straight line path, and thus its propagation path can be predefined; (5) a fixed time step approach is utilized to discrete the time derivative terms of hydro-fracking problem. All the reference parameters for the simplification in the simulation studies are listed in Tab. 1.

On the basis of the above assumptions, the algorithm of the transient, coupled, non-linear hydro-fracking problem is summarized as:

for each non-linear iteration loop, SVD method is adopted to separate the non-linear term $K^\delta(w^3)$ as $K^l(x)$ and $\phi^l(t)$. Then we use PGD method to get the separated representations of X and T for all modes. Here, alternating direction iteration method is used to get X and T for each enrichment step (or each mode). The detailed description is as follows:

Algorithm 1: The PGD algorithm of the 2D hydraulic fracturing problem

Input: $E, \nu, \sigma_H, \sigma_h$ and material parameters

Output: X_m, T_m

```

for  $\delta = 1; \delta \leq \max\delta$  do
    /* loop3, */
    compute  $K_{w^3}^\delta = \sum_l K^l(x)\phi^l(t)$  via SVD;
    solve for  $p^{\delta+1}$  using PGD. Find  $p^{\delta+1}$  such that;
    for  $m = 1; j \leq \maxModes$  do
        /* loop2, */
         $p = p_0$ ;
        for  $I = 1; I \leq \maxIter$  do
            /* loop1, */
            solve for  $X$ ;
            solve for  $T$ ;
        end
         $p^m = p^{m-1} + X_m T_m$ ;
    end
    return  $X_m, T_m$ ;
end

```

Remark:

1. For simplicity, fracture propagation path is predefined in the mesh. i.e., the same coordinate of x and y is occupied by two nodes on two fracture surfaces, but they have different node numbers. Thus it is not necessary to calculate the stress intensify factor and determine the crack tip direction, thus the singularity near the crack tips is not considered in this paper.
2. For simplicity, the coupled fracking problem is composed of 2D solid equation (Plane

strain) + 1D fluid equation. Without loss of generality, the same method can be extended into the case of 3D. Because the fracture width is very small, the fluid equation can be viewed as a 1D problem along the fracture length direction. Because the strain in the z -direction (fracture height) is very small, the stress equilibrium equation can be viewed as a 2D problem (Plane strain) [Yew and Weng (2014); Zlotnik, Díez, Modesto et al. (2015)].

Table 1: Reference parameters for the simplification in the simulation studies

| Reference parameters | Value |
|---|----------------------------|
| coordinates of two crack tips of predefined fracture | (-1,0), (1,0) |
| leak-off rate of fluid, C_L | 0 |
| element type of fluid pressure/hydro-fracture | line element (1D) |
| element type of rock matrix | quadrilateral element (2D) |
| maximum modes, m (Eq. (29)) | 10 (loop2) |
| maximum iteration times, p (Eq. (35)) | 5 (loop 3) |
| maximum nonlinear iteration times, δ (Eq. (59)) | 16 (loop1) |
| nonlinear iteration tolerance, ε (Eq. (35)) | 0.001 |
| iteration tolerance of SVD, l (Eq. (34)) | 1e-10 |
| time step, Δt (Eq. (54)) | 0.01 min |
| Mesh size, h | 0.25 m |

4 Numerical examples

4.1 Verification: compared with the results via FEM algorithm

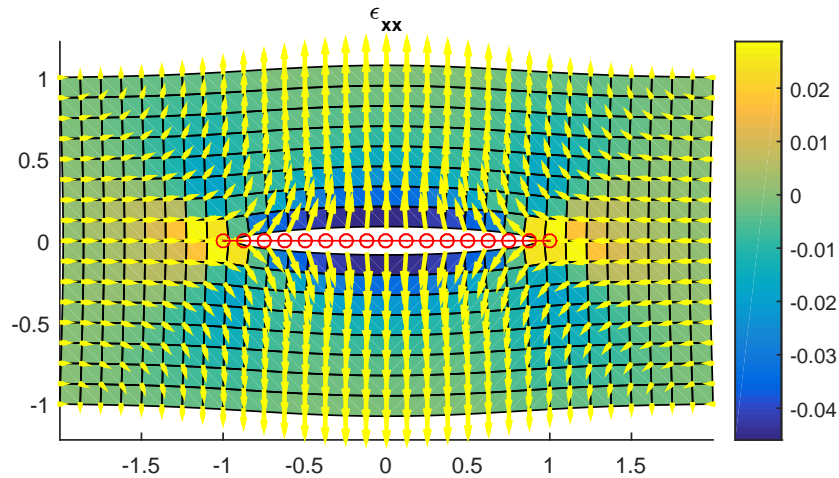


Figure 2: Results via FEM method. ε_{xx} denotes the displacement in x -axis direction

We use the same parameters and mesh sizes in Tab. 2 to compare the results via FEM method and PGD method respectively, as shown in Figs. 2 and 3. In addition, the reliability will be further revealed in the next subsection of convergence analysis. The numerical

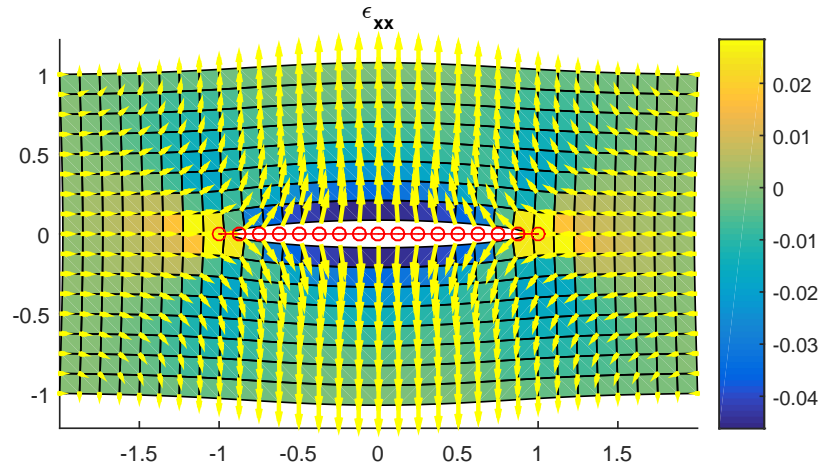


Figure 3: Results via PGD method. ϵ_{xx} denotes the displacement in x -axis direction

results of PGD match well with the results of FEM, which verify that PGD method has good numerical accuracy and is a reliable method, as shown in Fig. 4. Further, the calculation time via PGD algorithm is much less than that via FEM algorithm, shown in Tab. 3 (a computer with 16 GB memory and Intel 3.7 GHz CPU). It is observed that the average computational cost of PGD is approximate 10% of that FEM, which means that the computational efficiency of PGD is approximate ten times of that FEM. Therefore, PGD method is much faster than FEM method in simulating the hydraulic fracturing problem [González, Alfaro, Quesada et al. (2015); Zlotnik, Díez, Modesto et al. (2015); Tamellini, Le Maitre and Nouy (2014); Fjar, Holt, Raaen et al. (2008); Modesto, Zlotnik and Huerta (2015)].

Table 2: Input parameters of hydro-fracking model

| Input Parameter | Value |
|---------------------------------------|-----------|
| Young’s Modulus, E | 17 GPa |
| Poisson’s ratio, ν | 0.2 |
| Viscosity of fracturing fluid, μ | 1 mPa · s |
| Pore pressure, P_0 | 3.7 MPa |
| Maximum horizontal stress, σ_H | 2 MPa |
| Minimum horizontal stress, σ_h | 2 MPa |
| Injection time, t | 1 min |

4.2 Convergence analysis

The errors of fluid pressure in the hydro-fracture and fracture opening at different mesh sizes are respectively calculated. The corresponding results are shown in Figs. 5 and 6, respectively. The error is defined as follows:

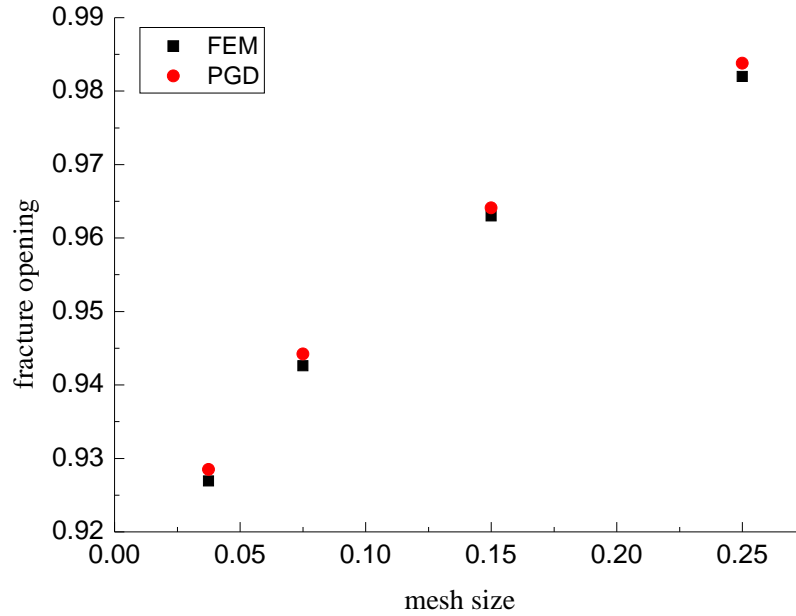


Figure 4: The solution comparison between PGD and FEM

Table 3: The comparison of simulation time between FEM and PGD

| Numerical method | Calculation time(s) | | | |
|------------------|---------------------|---------------|---------------|---------------|
| | mesh size h | mesh size h/2 | mesh size h/4 | mesh size h/8 |
| FEM | 14.41 | 56.63 | 481.59 | 803.63 |
| PGD | 3.63 | 5.22 | 7.17 | 47.58 |

$$error = \frac{\| X_h - X_{ref} \|}{max(X_{ref})} \quad (59)$$

where the reference solution is defined as the result that calculated on the finest mesh size; X_h denotes the pressure or fracture opening solution with different mesh sizes; and X_{ref} denotes the reference solution. As shown in the two figures, their solutions are stable because of the linear relationship between the errors and mesh size. Hence, Results show a very good convergence and accuracy towards the full finite element solution of the problem in terms of fracture opening and fluid pressure in the fracture.

4.3 Some numerical results via PGD algorithm

Fluid pressure and fracture opening distribution along the fracture nodes are shown in Figs. 7 and 8. Both of them have a maximum value at the center of fracture nodes, that are corresponding to the injection point, i.e., source term in the fluid pressure equation. With the increase of fracture length, the values of fracture opening and fluid pressure will become smaller and smaller. At the two fracture tips, their values of fracture opening and fluid pressure are both equal to zero. These simulation results have the same tendencies as the

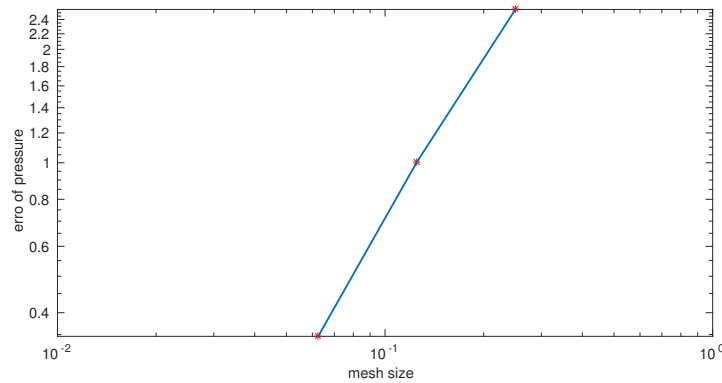


Figure 5: The double logarithmic curve between mesh size and error of fluid pressure

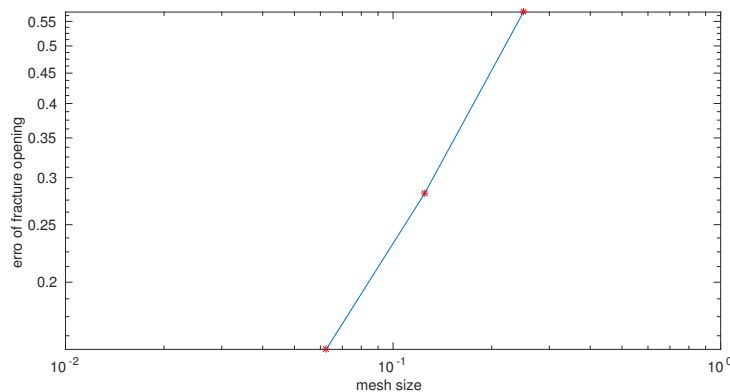


Figure 6: The double logarithmic curve between mesh size and error of fracture opening

published results [Yew and Weng (2014); Nolte and Economides (2000); Modesto, Zlotnik and Huerta (2015); Wang, Zhou, Ding et al. (2015)].

In future work, some key engineering and mechanical parameters, such as fluid viscosity, injection rate, Young's modulus, Poisson's ratio, and far-field stress, will be considered into the current PGD formulation, and try to solve the parametrized hydro-fracking equations.

5 Conclusions

1. In this work, PGD technique is applied to efficiently solve the transient, non-linear and coupled hydro-fracking problem in petroleum engineering.
2. Several numerical examples of hydro-fracking problem show that PGD solver can be smoothly used in most cases with good accuracy. Importantly, the PGD solution is much faster and more efficient than the full finite element solution.
3. The PGD strategy in this paper is quite different from the standard incremental time integration schemes. The number of non-linear iterations of the alternating direction algorithm rarely exceeds ten, while the modes N is often a few tens.

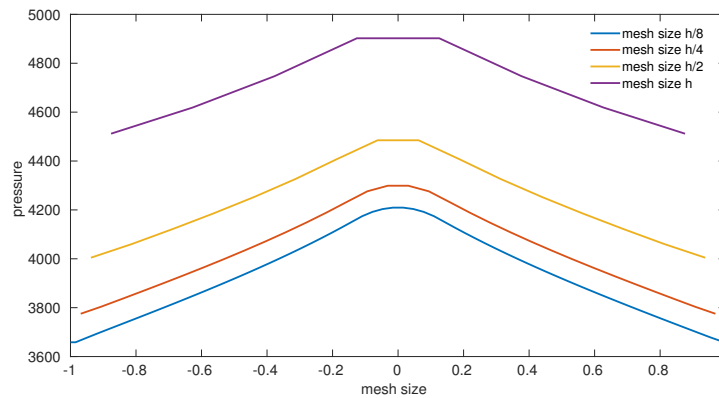


Figure 7: Fluid pressure distribution at all the fracture nodes (mesh size $h=0.25$)

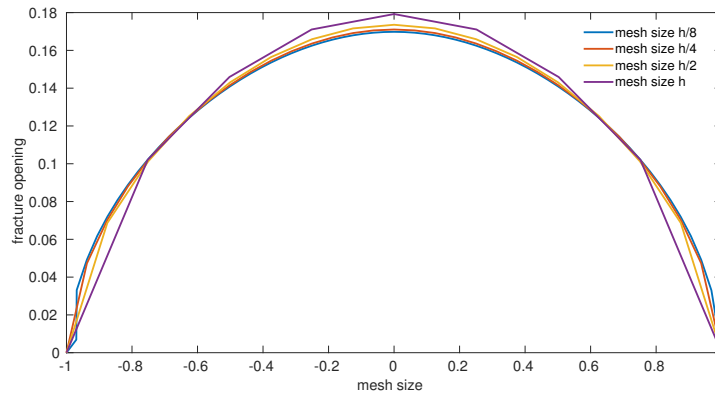


Figure 8: Fracture opening distribution at all the fracture nodes (mesh size $h=0.25$)

Acknowledgement: This work is financially supported by the National Science Foundation of China (Grant Nos. 51804033 and 51936001), China Postdoctoral Science and Foundation (Grant No. 2018M641254), Beijing Postdoctoral Research Foundation (2018-ZZ-045), the Project of Construction of Innovative Teams and Teacher Career Development for Universities and Colleges Under Beijing Municipality (Grant No. IDHT20170507) and Program of Great Wall Scholar (Grant No. CIT&TCD20180313) and Jointly Projects of Beijing Natural Science Foundation and Beijing Municipal Education Commission (Grant No. KZ201810017023).

Conflicts of Interest: The authors declare that they have no conflicts of interest to report regarding the present study.

References

- Adachi, J.; Siebrits, E.; Peirce, A.; Desroches, J.** (2007): Computer simulation of hydraulic fractures. *International Journal of Rock Mechanics and Mining Sciences*, vol. 44, no. 5, pp. 739-757.
- Aguado, J. V.; Huerta, A.; Chinesta, F.; Cueto, E.** (2015): Real-time monitoring

of thermal processes by reduced-order modeling. *International Journal for Numerical Methods in Engineering*, vol. 102, no. 5, pp. 991-1017.

Ammar, A. (2010): The proper generalized decomposition: a powerful tool for model reduction. *International Journal of Material Forming*, vol. 3, no. 2, pp. 89-102.

Chinesta, F.; Keunings, R.; Leygue, A. (2013): *The Proper Generalized Decomposition for Advanced Numerical Simulations: a Primer*. Springer International Publishing Cham Heidelberg New York Dordrecht London.

Chinesta, F.; Ladeveze, P.; Cueto, E. (2011): A short review on model order reduction based on proper generalized decomposition. *Archives of Computational Methods in Engineering*, vol. 18, no. 4, pp. 395.

Douillet-Grellier, T.; Pramanik, R.; Pan, K.; Albaiz, A.; Jones, B. D. et al. (2016): Mesh-free numerical simulation of pressure-driven fractures in brittle rocks. *SPE Hydraulic Fracturing Technology Conference*.

Fjar, E.; Holt, R. M.; Raaen, A. M.; Horsrud, P. (2008): Petroleum related rock mechanics. Elsevier. vol. 53.

González, D.; Alfaro, I.; Quesada, C.; Cueto, E.; Chinesta, F. (2015): Computational vademecums for the real-time simulation of haptic collision between nonlinear solids. *Computer Methods in Applied Mechanics and Engineering*, vol. 283, pp. 210-223.

Haddad, M.; Du, J.; Vidal-Gilbert, S. (2017): Integration of dynamic microseismic data with a true 3D modeling of hydraulic-fracture propagation in the vaca muerta shale. *SPE Journal*, vol. 22, no. 6, pp. 1-714.

Haddad, M.; Sepehrnoori, K. (2015): Integration of XFEM and CZM to model 3D multiple-stage hydraulic fracturing in quasi-brittle shale formations: solution-dependent propagation direction. *Proceedings of the AADE National Technical Conference and Exhibition, San Antonio, Texas, 8-9 April 2015*.

Henneron, T.; Clenet, S. (2015): Application of the pgd and deim to solve a 3-D non-linear magnetostatic problem coupled with the circuit equations. *IEEE Transactions on Magnetics*, vol. 52, no. 3, pp. 1-4.

Hunsweck, M. J.; Shen, Y.; Lew, A. J. (2013): A finite element approach to the simulation of hydraulic fractures with lag. *International Journal for Numerical and Analytical Methods in Geomechanics*, vol. 37, no. 9, pp. 993-1015.

Ji, L.; Settari, A.; Sullivan, R. B. (2009): A novel hydraulic fracturing model fully coupled with geomechanics and reservoir simulation. *SPE Journal*, vol. 14, no. 3, pp. 423-430.

Kumar, A.; Camilleri, D.; Brewer, M. (2016): Comparative analysis of dual continuum and discrete fracture simulation approaches to model fluid flow in naturally fractured, low-permeability reservoirs. *SPE Low Perm Symposium. Society of Petroleum Engineers*.

Ladevèze, P.; Passieux, J.-C.; Néron, D. (2010): The latin multiscale computational method and the proper generalized decomposition. *Computer Methods in Applied Mechanics and Engineering*, vol. 199, no. 21-22, pp. 1287-1296.

McClure, M. W.; Babazadeh, M.; Shiozawa, S.; Huang, J. (2016): Fully coupled hydromechanical simulation of hydraulic fracturing in 3D discrete-fracture networks. *SPE Journal*, vol. 21, no. 4, pp. 1-302.

- Miehe, C.; Mauthe, S.** (2016): Phase field modeling of fracture in multi-physics problems. part III. crack driving forces in hydro-poro-elasticity and hydraulic fracturing of fluid-saturated porous media. *Computer Methods in Applied Mechanics and Engineering*, vol. 304, pp. 619-655.
- Modesto, D.; Zlotnik, S.; Huerta, A.** (2015): Proper generalized decomposition for parameterized helmholtz problems in heterogeneous and unbounded domains: application to harbor agitation. *Computer Methods in Applied Mechanics and Engineering*, vol. 295, pp. 127-149.
- Nolte, K. G.; Economides, M. J.** (2000): *Reservoir Stimulation*. John Wiley & Sons Chichester New York.
- Pogacnik, J.; Elsworth, D.; O'Sullivan, M.; O'Sullivan, J.** (2016): A damage mechanics approach to the simulation of hydraulic fracturing/shearing around a geothermal injection well. *Computers and Geotechnics*, vol. 71, pp. 338-351.
- Secchi, S.; Schrefler, B.** (2012): A method for 3-D hydraulic fracturing simulation. *International Journal of Fracture*, vol. 178, no. 1-2, pp. 245-258.
- Shimizu, H.; Murata, S.; Ishida, T.** (2011): The distinct element analysis for hydraulic fracturing in hard rock considering fluid viscosity and particle size distribution. *International Journal of Rock Mechanics and Mining Sciences*, vol. 48, no. 5, pp. 712-727.
- Signorini, M.; Zlotnik, S.; Díez, P.** (2017): Proper generalized decomposition solution of the parameterized helmholtz problem: application to inverse geophysical problems. *International Journal for Numerical Methods in Engineering*, vol. 109, no. 8, pp. 1085-1102.
- Tamellini, L.; Le Maitre, O.; Nouy, A.** (2014): Model reduction based on proper generalized decomposition for the stochastic steady incompressible navier-stokes equations. *SIAM Journal on Scientific Computing*, vol. 36, no. 3, pp. A1089-A1117.
- Wang, D.; Zhou, F.; Ding, W.; Ge, H.; Jia, X. et al.** (2015): A numerical simulation study of fracture reorientation with a degradable fiber-diverting agent. *Journal of Natural Gas Science and Engineering*, vol. 25, pp. 215-225.
- Wang, W.; Shahvali, M.; Su, Y.** (2015): A semi-analytical fractal model for production from tight oil reservoirs with hydraulically fractured horizontal wells. *Fuel*, vol. 158, pp. 612-618.
- Yan, C.; Zheng, H.** (2017): Fdem-flow3d: A 3D hydro-mechanical coupled model considering the pore seepage of rock matrix for simulating three-dimensional hydraulic fracturing. *Computers and Geotechnics*, vol. 81, pp. 212-228.
- Yew, C. H.; Weng, X.** (2014): *Mechanics of Hydraulic Fracturing*. Gulf Professional Publishing, Waltham, USA.
- Yuan, B.; Zheng, D.; Moghanloo, R. G.; Wang, K.** (2017): A novel integrated workflow for evaluation, optimization, and production prediction in shale plays. *International Journal of Coal Geology*, vol. 180, pp. 18-28.
- Zlotnik, S.; Díez, P.; Modesto, D.; Huerta, A.** (2015): Proper generalized decomposition of a geometrically parametrized heat problem with geophysical applications. *International Journal for Numerical Methods in Engineering*, vol. 103, no. 10, pp. 737-758.